Desalination and Water Treatment
www.deswater.com

doi: 10.1080/19443994.2015.1086895

57 (2016) 17220–17229
August

Taylor & Francis
Taylor & Francis Group

Synthesis of CuO–NiO nanocomposite and dye adsorption modeling using artificial neural network

Niyaz Mohammad Mahmoodi*, Zahra Hosseinabadi-Farahani, Farzaneh Bagherpour, Mohammad Reza Khoshrou, Hooman Chamani, Fahimeh Forouzeshfar

Department of Environmental Research, Institute for Color Science and Technology, Tehran, Iran, Tel. +98 21 22969771; Fax: +98 21 22947537; emails: mahmoodi@icrc.ac.ir, nm_mahmoodi@aut.ac.ir (N.M. Mahmoodi), zahrahof80@gmail.com (Z. Hosseinabadi-Farahani), farzan.1362@yahoo.com (F. Bagherpour), m.khoshroo@znu.ac.ir (M.R. Khoshrou), chamani.hooman@yahoo.com (H. Chamani), f.forouzesh90@yahoo.com (F. Forouzeshfar)

Received 7 January 2015; Accepted 14 August 2015

ABSTRACT

In this paper, CuO–NiO nanocomposite was synthesized and used to remove cationic dyes from wastewater. The scanning electron microscopy, Fourier transform infrared spectroscopy, and X-ray diffraction were used to characterize the nanocomposite. Basic Red 18 (BR18) and Basic Blue 41 (BB41) were used as cationic dyes. Artificial neural network (ANN) model was used to predict the efficiency of dye removal. The effect of adsorbent dosage and dye concentration on dye removal was evaluated. The studied operating variables were used as the input to the constructed neural network to predict the dye removal at any time as the output or the target. The backpropagation neural network with Levenberg–Marquardt training algorithm was used to predict adsorption efficiency with a tangent sigmoid transfer function (tansig) at hidden layer and a linear transfer function (purelin) at output layer. The results showed the dye adsorption kinetics followed pseudo-second-order kinetics model. Dye removal isotherm was fitted with Temkin and Freundlich models for BB41 and BR18, respectively. The linear regression between the network outputs and the corresponding targets were proven to be satisfactory with a correlation coefficient. In addition, ANN modeling could effectively predict and simulate the behavior of the process.

Keywords: Synthesis; CuO–NiO nanocomposite; Dye removal modeling; Artificial neural network; Wastewater

1. Introduction

Dyes are organic pollutants originating from many industries, such as textile, rubber, paper, leather, plastics, cosmetics, and food [1–14]. It is recognized that public perception of water quality is greatly influenced by the color. The presence of very small amounts of dyes in water is highly visible and undesirable [6,7]. In addition, dye in water interferes with light penetration and thus reduces the photosynthesis in aquatic plants which destroys aquatic ecosystems [6,8–10]. Wastewater containing dyes is difficult to treat because most dyes are resistant to biological degradation and oxidation [6,12–14]. Various methods for dye contaminated waters with varying degrees of advantage have been applied, such as coagulation/flocculation, chemical

*Corresponding author.

oxidation, ion exchange, irradiation, membrane filtration, sedimentation, solvent extraction, reverse osmosis, biological treatment, photocatalytic degradation [15–20], electrochemical treatment, and adsorption [4,9]. Among these methods, the adsorption process has proved to be a more powerful technique due to its simplicity, low cost, ease of operation, flexibility, minimum sludge production, and insensitivity to specific toxic substances [10,21,22]. For this purpose, many adsorbents including activated carbon, synthetic polymer, etc. were investigated, but they have some problems, such as high cost and time-consuming method for synthesis [10]. Thus, the synthesis of an adsorbent with low cost and good capacity for adsorption in a short time is preferred.

Artificial neural networks (ANNs) have the ability of learning, simulation, and prediction of data. The inspiration of using neural network came from the biology of human brain. ANNs are now commonly used in many research areas of science and engineering and represent a set of methods that may be useful in predicting water quality using water treatment parameters. Unlike traditional statistical and differential equation approaches, ANNs are considered to be a powerful data modeling tool, as it can capture and implicitly represent complex relationships with many variables, such as the input/output variables. The neural networks are able to represent both linear and nonlinear relationships and are ingenious to learn the relationships directly from data used for training the network. In addition, ANNs do not require the mathematical description of the phenomena involved in the process. The network consists of numerous individual processing units called neurons which are commonly interconnected in a variety of structures. The strength of these interconnections is determined by the weight associated with neurons. The multilayer feed-forward net is a parallel interconnected structure consisting of input layer and includes independent variables, number of hidden layers, and output layer [23–41].

A literature review showed that ANN modeling of dye removal using CuO–NiO nanocomposite as an adsorbent was not studied. In this paper, a simple and low-cost procedure was reported for producing CuO–NiO nanocomposite as an inorganic adsorbent. The characteristics of the nanocomposite were studied using scanning electron microscopy (SEM), Fourier transform infrared (FTIR) spectroscopy and X-ray diffraction (XRD). Basic Red 18 (BR18) and Basic Blue 41 (BB41) were used. ANN model was used to predict the efficiency of dye removal from aqueous solution. The effect of adsorbent dosage and dye concentration on dye removal was evaluated. The kinetic and isotherm of adsorption process was investigated.

2. Experimental

2.1. Materials and methods

Copper sulfate·$5H_2O$ powder, nickel sulfate·$6H_2O$ powder, and sodium hydroxide were purchased from Merck (Germany). Two cationic dyes (BB41 and BR18) were used as model dyes. The chemical structure of dyes is shown in Fig. 1.

2.2. Preparation of CuO–NiO nanocomposite and characterization

Copper sulfate (1 g) and nickel sulfate (1 g) were added to 90 mL of deionized water containing sodium hydroxide (1 g). The solution was magnetically stirred for 3 h. The bottle containing the solution was sealed and placed at 120℃ in an oven for 24 h. Then, the supernatant was discarded and residue solid was washed with deionized water. The precipitate was dried in an oven at 120℃. The functional groups of nanocomposite were studied using FTIR (Perkin-Elmer spectrophotometer spectrum one) in the range 4,000–450 cm^{-1}. The morphological structure of nanocomposite was examined by SEM (LEO 1455VP scanning electron microscope). The powder XRD measurement was recorded by XRD model Siemens D-5000 diffractometer with Cu Kα radiation at room temperature.

2.3. Adsorption procedure

Nanocomposite was added to dye solution (250 mL) and the solution was stirred. The solution samples were withdrawn at certain time intervals during the adsorption process. The absorbance change of samples was monitored and determined. At the end

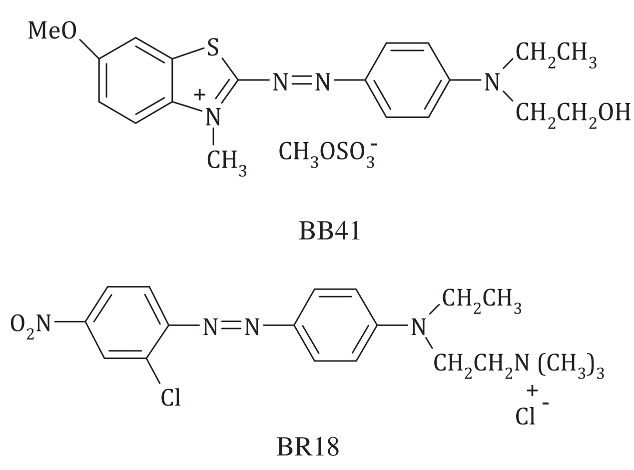

Fig. 1. The chemical structure of dyes.

of dye adsorption process, samples were centrifuged and their absorbance was determined. UV–vis Spectrophotometer (Perkin-Elmer Lambda 25 Spectrophotometer) was used for absorbance measurements of samples. Maximum wavelength for absorbance measurement of BR18 and BB41 was 488 and 580 nm, respectively.

The effect of adsorbent dosage on dye removal was investigated by contacting 250 mL of dye solution (20 mg/mL) at room temperature for 60 min. Different amounts of nanocomposite (0.1–1.6 g/L) were used.

The effect of initial dye concentration (20–80 mg/L) on dye removal was studied by contacting 250 mL of dye solution with nanocomposite at room temperature for 60 min.

3. Result and discussion

3.1. Characterization

In order to investigate the functional group of CuO–NiO nanocomposite, FTIR in the range 450–4,000 cm^{-1} was studied. FTIR spectrum of the synthesized adsorbent is shown in Fig. 2. The peak at 3,437 cm^{-1} is attributed to hydroxyl group stretching [42,43]. The sharp band at 3,642 cm^{-1} is assigned to isolated hydroxyl groups [42]. The band at 1,632 cm^{-1} is attributed to bending vibration of water molecule [42–46]. The bands at 615 and 499 cm^{-1} are due to Ni–O–H bending and Ni–O stretching, respectively [42,47,48]. The band assigned at 530–440 cm^{-1} of the mixed oxides may be attributed to the M–O (Cu–O) vibration [43]. The peak at 1,011 cm^{-1} is related to bending vibration of OH.

SEM is a suitable tool for characterization of shape and morphology of material surface. FESEM and SEM images of CuO–NiO nanocomposite are shown in Fig. 3. As it is evident in the image, nanoparticles have a flake shape with thickness <50 nm.

Fig. 4 shows the XRD pattern of CuO–NiO nanocomposite. NiO diffraction peaks and CuO diffraction peaks are clearly observed, indicating a mixture of CuO and NiO [43,49–51].

3.2. ANN modeling of dye removal

To predict the dye removal in this study, Neural Network Toolbox V4.0 of MATLAB 9 mathematical software was used. A three-layer ANN with tangent sigmoid transfer functions with backpropagation algorithm was designed. The data gathered from batch dye-removal experiments were divided into input matrix and target matrix. This model consisted of an input layer, a hidden layer, and an output layer. An ANN was trained to perform a particular (activation) function by adjusting the values of the connections (weights) between elements (neurons). The activation function produced the output using a sum weight of each neuron (Wi) and a bias (bi) that a constant weight of a neuron representing the generalization error. The performance of the ANN model was statistically measured by the mean square error (MSE) and regression coefficient, which are calculated with the experimental values and network predictions. These calculations are used as a criterion for model adequacy obtained as follows [23–41]:

$$\mathrm{MSE} = \frac{\sum_{i=1}^{N}\left(y_{\mathrm{pred}} - y_{\mathrm{exp}}\right)^2}{N} \quad (1)$$

$$R^2 = 1 - \frac{\sum_{i=1}^{N}\left(y_{\mathrm{pred}} - y_{\mathrm{exp}}\right)^2}{\sum_{i=1}^{N}\left(y_{\mathrm{exp}} - y_{\mathrm{m}}\right)^2} \quad (2)$$

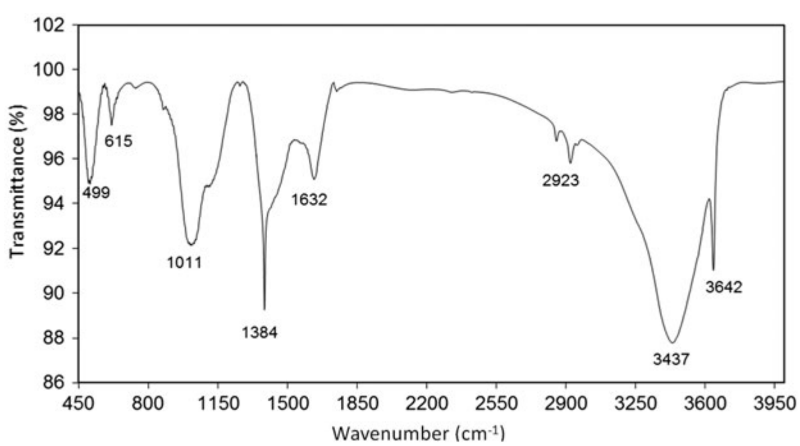

Fig. 2. FTIR spectrum of CuO–NiO nanocomposite.

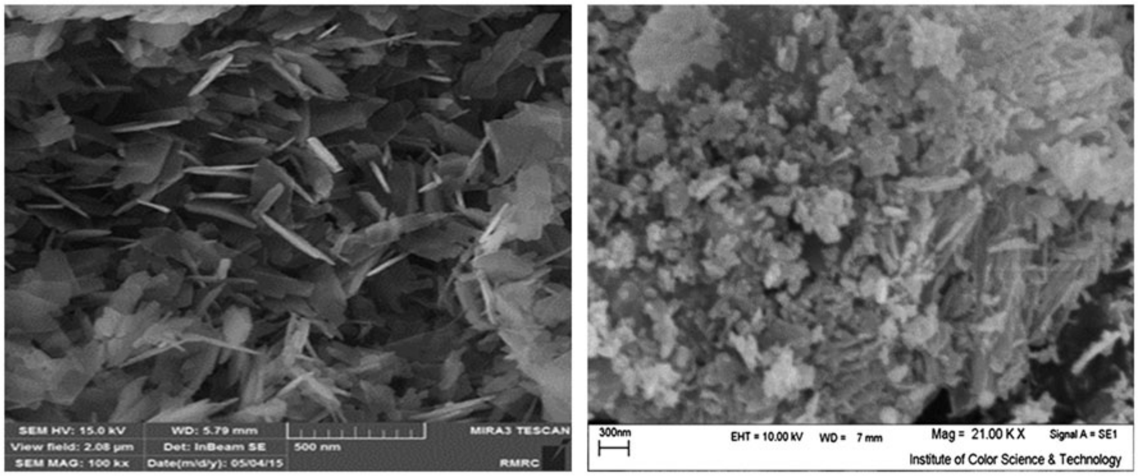

Fig. 3. Images of CuO–NiO nanocomposite (a) FESEM (left) and (b) SEM (right).

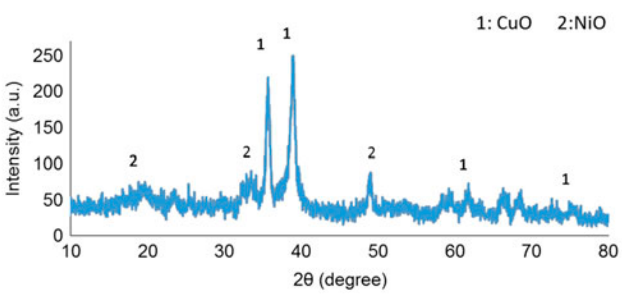

Fig. 4. XRD pattern of CuO–NiO nanocomposite.

where N, y_{pred}, y_{exp}, y_{m} and i are the number of data points, the network prediction, the experimental response, the average of actual values, and an index of data, respectively.

The optimum number of neurons was determined based on the minimum value of MSE of the training and prediction set. The optimization was done using Levenberg–Marquardt algorithm as a training algorithm and with varying neuron number. Fig. 5 shows the relationship between number of neurons and MSE.

A regression analysis of the network response between ANN outputs and the corresponding targets was performed. The graphical output of the network plotted vs. the targets as open circles is illustrated in Fig. 6. Taking into account the nonlinear dependence of the data, linear regression shows a good agreement between ANN outputs (predicted data) and the corresponding targets (experimental data). The best linear fit was indicated by a solid line and R^2 values.

Dye removal at different CuO–NiO nanocomposite dosages (g) is shown in Fig. 7. The increase in dye adsorption with adsorbent dosage can be attributed to

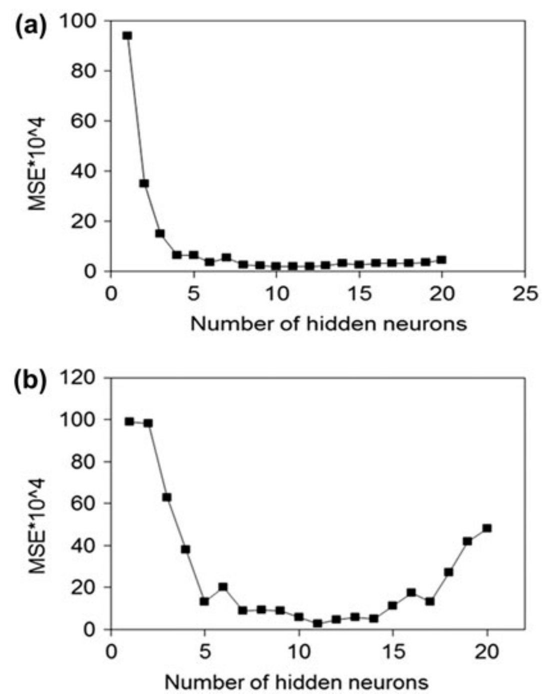

Fig. 5. The relationship between number of neurons and MSE (a) BB41 and (b) BR18.

the increase in adsorbent surface and availability of more adsorption sites. However, if the adsorption capacity was expressed in mg/g of material, the capacity decreased with the increasing amount of the adsorbent. It can be attributed to overlapping or aggregation of adsorption sites resulting in a decrease in total adsorbent surface area available to the dye. In addition, Fig. 7 shows a comparison between the ANN model predictions and the experimental data as

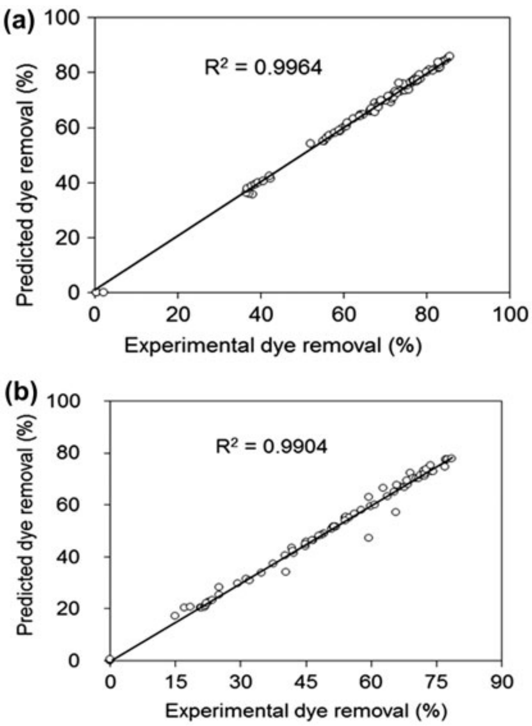

Fig. 6. The graphical output of the network outputs plotted vs. the targets as open circles (a) BB41 and (b) BR18.

a function of adsorbent dosage. It can be seen that the ANN model satisfactorily predicts the trend of the experimental data.

The effect of initial dye concentration on dye removal were studied. The results are shown in Fig. 8. It is obvious that the higher the initial dye concentration, the lower the percentage of dye adsorbed. The amount of the dye adsorbed onto CuO–NiO nanocomposite increases with an increase in the initial dye concentration of solution if the amount of adsorbent is kept unchanged due to the increase in the driving force of the concentration gradient with the higher initial dye concentration. The adsorption of dye by the adsorbent is very intense and reaches equilibrium very quickly at low initial concentration. At a fixed CuO–NiO nanocomposite dosage, the amount of dye adsorbed increased with increasing concentration of solution, but the percentage of adsorption decreased. In other words, the residual dye concentration will be higher for higher initial dye concentrations [52]. In addition, the experimental data and ANN calculated outputs for various initial dye concentration values are shown in Fig. 8. It can be seen that the ANN model shows a good performance on prediction of the experimental data.

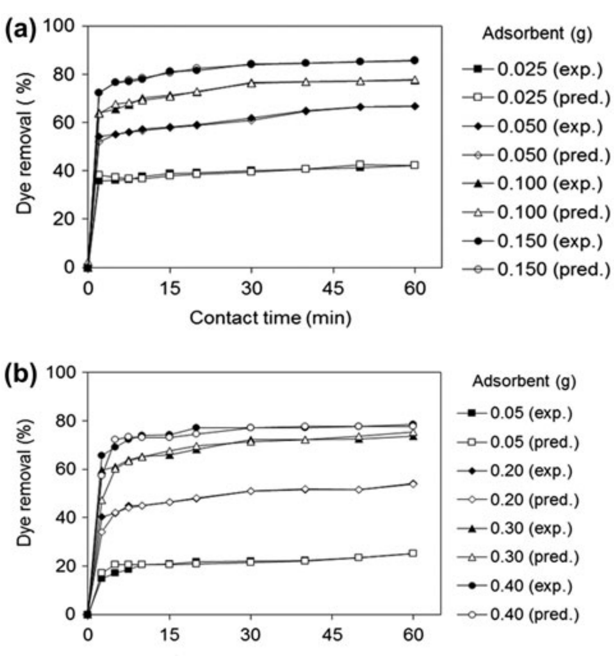

Fig. 7. ANN predicted outputs (pred.) and experimental data (exp.) of dye removal at different adsorbent dosages (dye: 20 mg/L and natural pH 6) (a) BB41 and (b) BR18.

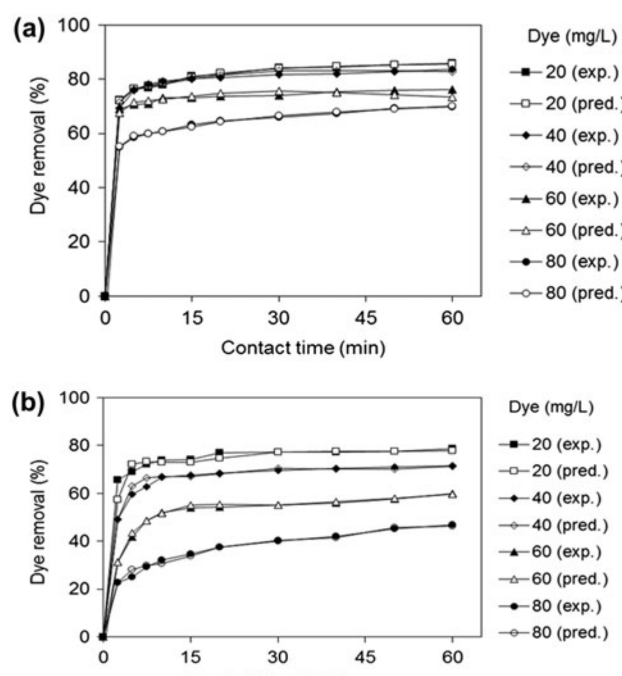

Fig. 8. ANN predicted outputs (pred.) and experimental data (exp.) of dye removal at different initial dye concentrations (adsorbent dosage: 0.15 g for BB41 and 0.4 g for BR18 and natural pH 6) (a) BB41 and (b) BR18.

3.3. Adsorption kinetics

Several models can be used to express the mechanism of adsorption onto an adsorbent. In order to investigate the mechanism of adsorption, characteristic constants of sorption were determined using pseudo-first-order, pseudo-second-order, and intraparticle diffusion models [53,54]. A linear form of pseudo-first-order model is [55]:

$$\log(q_e - q_t) = \log(q_e) - (k_1/2.303)t \tag{3}$$

where q_e, q_t, and k_1 are the amount of adsorbed dye at equilibrium (mg/g), the amount of adsorbed dye at time t (mg/g), and the equilibrium rate constant of pseudo-first-order kinetics (1/min), respectively.

To understand the applicability of the pseudo-first-order for dye adsorption onto CuO–NiO nanocomposite at different adsorbent dosages, linear plots of log $(q_e - q_t)$ vs. contact time (t) are plotted (Fig. 9). The values of k_1, R^2, and the calculated q_e ($(q_e)_{cal}$) are shown in Table 1.

Linear form of pseudo-second-order model was illustrated as [55]:

$$t/q_t = 1/k_2 q_e^2 + (1/q_e)t \tag{4}$$

where k_2 is the equilibrium rate constant of pseudo-second-order (g/mg min).

To understand the applicability of the pseudo-second-order for dye adsorption onto the nanocomposite at different adsorbent dosages, linear plots of t/q_t vs. contact time (t) are plotted (Fig. 10). The values of k_2, R^2, and $(q_e)_{cal}$ are shown in Table 1.

The possibility of intraparticle diffusion resistance affecting adsorption was explored using the intraparticle diffusion model as [54,55]:

$$q_t = k_p t^{1/2} + I \tag{5}$$

where k_p and I are the intraparticle diffusion rate constant and intercept, respectively.

To understand the applicability of the intraparticle diffusion for dye adsorption onto the nanocomposite at different adsorbent dosages, linear plots of q_t vs. $t^{1/2}$ are plotted (Fig. 11). The values of k_p, R^2, and I are shown in Table 1.

The R^2 values showed that dye adsorption by CuO–NiO nanoadsorbent did not follow pseudo-first-order and intraparticle diffusion kinetics (Table 1). The linearity between the t/q_t against t and the R^2 values show that the kinetics of dye removal followed pseudo-second-order. In addition, the results obtained for ANN modeling were used to calculate the adsorption kinetic (Table 1). It is shown that the predictions of the designed ANN models are in close agreement with the experimental data.

3.4. Adsorption isotherm

Several isotherms such as Langmuir, Freundlich, and Temkin models were investigated in detail [56–60]. The Langmuir equation investigates the interaction between the adsorbent and the adsorbate as a linear, reversible, and monolayer chemical reaction. This model assumes that the adsorbent surface is completely homogeneous and each adsorbent site can bind a maximum of one adsorbate molecule. In addition, there are no interactions between molecules of the adsorbate. The Langmuir equation can be written as follows:

$$C_e/q_e = 1/K_L Q_0 + C_e/Q_0 \tag{6}$$

where C_e, K_L, and Q_0 are the equilibrium concentration of dye solution (mg/L), the Langmuir constant (L/g), and the maximum adsorption capacity (mg/g), respectively.

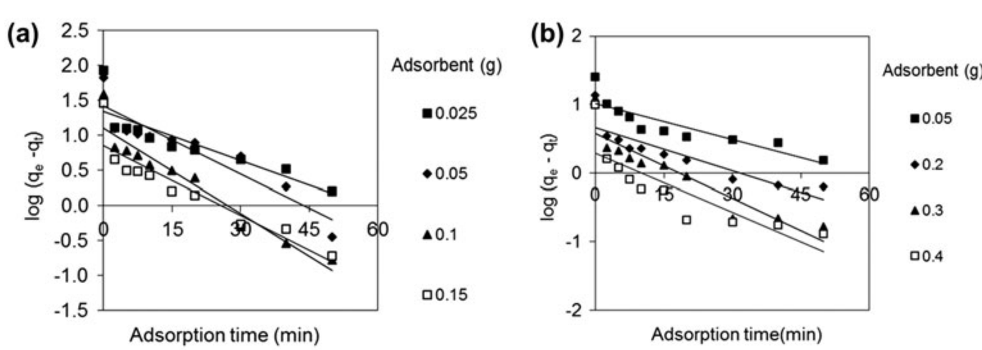

Fig. 9. Pseudo-first-order kinetics of dye removal by the nanocomposite (a) BB41 and (b) BR18.

Table 1
Linearized kinetics coefficients of dye removal using nanostructure at different adsorbent dosages

Data	Dye	Adsorbent (g)	$(q_e)_{exp}$	Pseudo-first-order			Pseudo-second-order			Intraparticle diffusion		
				$(q_e)_{cal}$	k_1	R^2	$(q_e)_{cal}$	k_2	R^2	k_p	I	R^2
Experimental data	BB41	0.0250	84	22	0.0541	0.7538	85	0.0096	0.9993	2.1577	68	0.9713
		0.0500	67	26	0.0746	0.8567	68	0.0080	0.9983	2.2010	50	0.9843
		0.1000	39	13	0.0937	0.9201	40	0.0213	0.9997	1.1673	31	0.9336
		0.1500	29	7	0.0762	0.8480	29	0.0374	0.9999	0.6892	24	0.9192
	BR18	0.0500	25	10	0.0405	0.7578	25	0.0146	0.9954	1.3363	15	0.8737
		0.2000	14	4	0.0479	0.7762	14	0.0389	0.9984	0.5201	10	0.9611
		0.3000	12	4	0.0723	0.8473	12	0.0599	0.9996	0.3926	9	0.9392
		0.4000	10	2	0.0656	0.7114	10	0.1399	0.9999	0.2228	8	0.8021
Predicted data by ANN	BB41	0.0250	84	21	0.052	0.7930	85	0.0110	0.9980	6.7000	44	0.4590
		0.0500	67	29	0.0812	0.8970	68	0.0096	0.9970	5.7300	31	0.5650
		0.1000	39	10	0.0670	0.8740	40	0.0260	0.9990	3.1890	20	0.5100
		0.1500	29	7	0.0790	0.8970	29	0.0520	0.9998	2.3301	15	0.4660
	BR18	0.0500	25	9	0.0340	0.7290	25	0.0180	0.9910	2.0960	9	0.5720
		0.2000	13	4	0.0440	0.7900	14	0.0450	0.9980	1.2480	6	0.6440
		0.3000	13	4	0.0520	0.8400	13	0.0570	0.9990	1.1570	5	0.6200
		0.4000	10	2	0.0980	0.8700	10	0.1520	0.9990	0.8220	5	0.4850

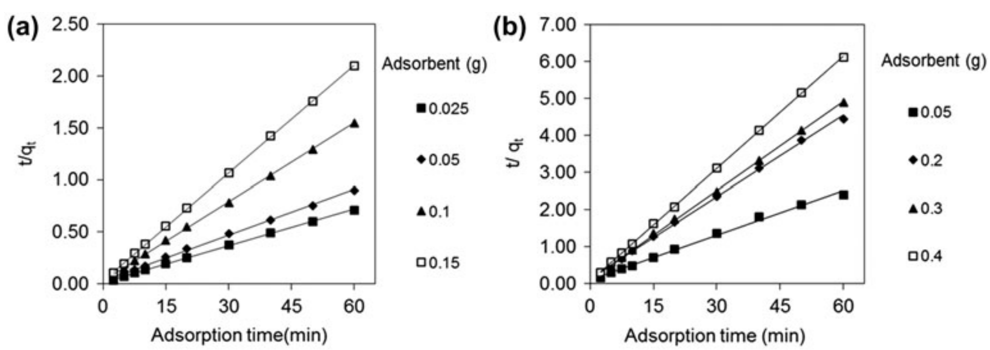

Fig. 10. Pseudo-second-order kinetics of dye removal by the nanocomposite (a) BB41 and (b) BR18.

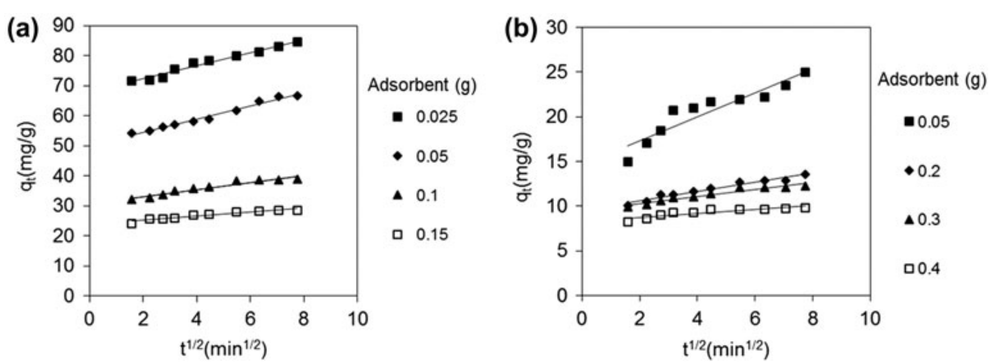

Fig. 11. Intraparticle diffusion kinetics of dye removal by the nanocomposite (a) BB41 and (b) BR18.

Table 2
Linearized isotherm coefficients of dye removal using CuO–NiO nanocomposite at different adsorbent dosages

	Langmuir			Freundlich			Temkin		
Data	Q_0	K_L	R^2	K_F	$1/n$	R^2	K_T	B_1	R^2
Experimental data	BB41								
	263	0.0428	0.6613	12	0.8121	0.9572	1.5300	42	0.9630
	BR18								
	55	0.0471	0.5014	4	0.6664	0.8898	1.8700	11	0.8413
Predicted data by ANN	BB41								
	278	0.0399	0.6520	12	0.8230	0.9581	1.5700	43	0.9690
	BR18								
	55	0.0470	0.450	4	0.6500	0.8480	1.8300	11	0.8150

The Freundlich isotherm assumes that the adsorbent surface is a heterogeneous surface with a non-uniform distribution of heat of adsorption over the surface. The Freundlich isotherm can be expressed by:

$$\log q_e = \log K_F + (1/n) \log C_e \tag{7}$$

where K_F is adsorption capacity at unit concentration and $1/n$ is the adsorption intensity. The $1/n$ values indicate the type of isotherm to be irreversible ($1/n = 0$), favorable ($0 < 1/n < 1$), and unfavorable ($1/n > 1$).

The adsorption in Temkin isotherm is characterized by a uniform distribution of binding energies, up to some maximum binding energy. The Temkin isotherm is given as:

$$q_e = B_1 \ln K_T + B_1 \ln C_e \tag{8}$$

where K_T is the equilibrium binding constant (L/mol) corresponding to the maximum binding energy and constant B_1 (RT/b) is related to the heat of adsorption. In addition, R and T are the gas constant (8.314 J/mol K) and the absolute temperature (K), respectively.

To study the applicability of the Langmuir, Freundlich, and Temkin isotherms for the dye adsorption onto CuO–NiO nanocomposite at different adsorbent dosages, linear plots of C_e/q_e against C_e, log q_e vs. log C_e, and q_e vs. ln C_e are plotted.

The Q_0, K_L, K_F, $1/n$, K_T, B_1, and R^2 (correlation coefficient) are given in Table 2. The Temkin isotherm is found to fit quite well with the experimental data for BB41 in accordance with the linear correlation coefficient. The R^2 values for BR18 indicate that the Freundlich isotherm is most appropriate for adsorption of this dye onto CuO–NiO nanocomposite. In addition, the results obtained for ANN modeling were used to calculate the adsorption isotherm (Table 2). The predictions of the designed ANN models are in close agreement with the experimental data.

4. Conclusion

In this study, adsorption process as a low-cost, simple, and efficient method was applied to remove cationic dyes from wastewater. CuO–NiO nanocomposite as an adsorbent was synthesized. The adsorbent was characterized with SEM, FTIR, and XRD. The result of adsorption process showed that CuO–NiO is a suitable adsorbent for cationic dye removal. The optimum adsorbent dosage and dye concentration were obtained. The results of kinetic studies revealed that adsorption of BB41 and BR18 onto CuO–NiO nanocomposite involved pseudo-second-order model. The equilibrium data showed that the experimental data were correlated reasonably well by Temkin isotherm model for BB41 and Freundlich isotherm model for BR18. ANN predicted results are very close to the experimental results with good correlation coefficient. The results showed that ANN modeling could effectively simulate and predict the behavior of the process.

References

[1] N.M. Mahmoodi, N.Y. Limaee, M. Arami, S. Borhany, M. Mohammad-Taheri, Nanophotocatalysis using nanoparticles of titania: Mineralization and finite element modelling of Solophenyl dye decolorization, J. Photochem. Photobiol., A: Chem. 189 (2007) 1–6.
[2] N.M. Mahmoodi, Manganese ferrite nanoparticle: Synthesis, characterization and photocatalytic dye degradation ability, Desalin. Water Treat. 53 (2015) 84–90.

[3] N.M. Mahmoodi, M. Arami, J. Zhang, Preparation and photocatalytic activity of immobilized composite photocatalyst (titania nanoparticle/activated carbon), J. Alloys Compd. 509 (2011) 4754–4764.
[4] M.T. Yagub, T.K. Sen, S. Afroze, H.M. Ang, Dye and its removal from aqueous solution by adsorption: A review, Adv. Colloid Interface Sci. 209 (2014) 172–184.
[5] N.M. Mahmoodi, Dendrimer functionalized nanoarchitecture: Synthesis and binary system dye removal, J. Taiwan Inst. Chem. Eng. 45 (2014) 2008–2020.
[6] S. Zhu, S. Jiao, Z. Liu, G. Pang, S. Feng, High adsorption capacity for dye removal by CuZn hydroxyl double salts, Environ. Sci.: Nano 1 (2014) 172–180.
[7] L. Zhou, C. Gao, W. Xu, Magnetic dendritic materials for highly efficient adsorption of dyes and drugs, ACS Appl. Mater. Interfaces 2 (2010) 1483–1491.
[8] N.M. Mahmoodi, Synthesis of magnetic carbon nanotube and photocatalytic dye degradation ability, Environ Monit. Assess. 186 (2014) 5595–5604.
[9] Q. Wu, C. Feng, C. Wang, Z. Wang, A facile one-pot solvothermal method to produce superparamagnetic graphene-Fe_3O_4 nanocomposite and its application in the removal of dye from aqueous solution, Colloids Surf., B 101 (2013) 210–214.
[10] H. Sun, L. Cao, L. Lu, Magnetite/reduced graphene oxide nanocomposites: One step solvothermal synthesis and use as a novel platform for removal of dye pollutants, Nano Res. 4 (2011) 550–562.
[11] N.M. Mahmoodi, R. Salehi, M. Arami, Binary system dye removal from colored textile wastewater using activated carbon: Kinetic and isotherm studies, Desalination 272 (2011) 187–195.
[12] J. Ma, F. Yu, L. Zhou, L. Jin, M. Yang, J. Luan, Y. Tang, H. Fan, Z. Yuan, J. Chen, Enhanced adsorptive removal of methyl orange and methylene blue from aqueous solution by alkali-activated multiwalled carbon nanotubes, ACS Appl. Mater. Interfaces 4 (2012) 5749–5760.
[13] C. Wang, C. Feng, Y. Gao, X. Ma, Q. Wu, Z. Wang, Preparation of a graphene-based magnetic nanocomposite for the removal of an organic dye from aqueous solution, Chem. Eng. J. 173 (2011) 92–97.
[14] B. Yang, Y. Guo, S. Zhang, T. Wen, C. Zhao, Synthesis of graphene by microwave irradiation for dye adsorption, RSC Adv. 4 (2014) 64771–64780.
[15] A. Nezamzadeh-Ejhieh, S. Hushmandrad, Solar photodecolorization of methylene blue by CuO/X zeolite as a heterogeneous catalyst, Appl. Catal., A 388 (2010) 149–159.
[16] N.M. Mahmoodi, Binary catalyst system dye degradation using photocatalysis, Fiber. Polym. 15 (2014) 273–280.
[17] N.M. Mahmoodi, Photocatalytic ozonation of dyes using multiwalled carbon nanotube, J. Mol. Catal. A: Chem. 366 (2013) 254–260.
[18] N.M. Mahmoodi, Photodegradation of dyes using multiwalled carbon nanotube and ferrous ion, J. Environ. Eng. 139 (2013) 1368–1374.
[19] N.M. Mahmoodi, Zinc ferrite nanoparticle as a magnetic catalyst: Synthesis and dye degradation, Mater. Res. Bull. 48 (2013) 4255–4260.
[20] N.M. Mahmoodi, Photocatalytic degradation of dyes using carbon nanotube and titania nanoparticle, Water Air Soil Poll. 224 (2013) 1612–1619.
[21] X. He, K.B. Male, P.N. Nesterenko, D. Brabazon, B. Paull, J.H.T. Luong, Adsorption and desorption of methylene blue on porous carbon monoliths and nanocrystalline cellulose, ACS Appl. Mater. Interfaces 5 (2013) 8796–8804.
[22] L. Sun, H. Yu, B. Fugetsu, Graphene oxide adsorption enhanced by *in situ* reduction with sodium hydrosulfite to remove acridine orange from aqueous solution, J. Hazard. Mater. 203–204 (2012) 101–110.
[23] K. Yetilmezsoy, S. Demirel, Artificial neural network (ANN) approach for modeling of Pb(II) adsorption from aqueous solution by Antep pistachio (*Pistacia Vera* L.) shells, J. Hazard. Mater. 153 (2008) 1288–1300.
[24] A.R. Khataee, M.B. Kasiri, Artificial neural networks modeling of contaminated water treatment processes by homogeneous and heterogeneous nanocatalysis, J. Mol. Catal. A: Chem. 331 (2010) 86–100.
[25] E.S. Elmolla, M. Chaudhuri, M.M. Eltoukhy, The use of artificial neural network (ANN) for modeling of COD removal from antibiotic aqueous solution by the Fenton process, J. Hazard. Mater. 179 (2010) 127–134.
[26] E. Oguz, M. Ersoy, Removal of Cu^{2+} from aqueous solution by adsorption in a fixed bed column and neural network modelling, Chem. Eng. J. 164 (2010) 56–62.
[27] Y.El. Hamzaoui, J.A. Hernández, S. Silva-Martínez, A. Bassam, A. Alvarez, C. Lizama-Bahena, Optimal performance of COD removal during aqueous treatment of alazine and gesaprim commercial herbicides by direct and inverse neural network, Desalination 277 (2011) 325–337.
[28] A. Çelekli, F. Geyik, Artificial neural networks (ANN) approach for modeling of removal of Lanaset Red G on Chara contraria, Bioresour. Technol. 102 (2011) 5634–5638.
[29] A. Çelekli, S.S. Birecikligil, F. Geyik, H. Bozkurt, Prediction of removal efficiency of Lanaset Red G on walnut husk using artificial neural network model, Bioresour. Technol. 103 (2012) 64–70.
[30] L. Cavas, Z. Karabay, H. Alyuruk, H. Doğan, G.K. Demir, Thomas and artificial neural network models for the fixed-bed adsorption of methylene blue by a beach waste *Posidonia oceanica* (L.) dead leaves, Chem. Eng. J. 171 (2011) 557–562.
[31] N. Prakash, S.A. Manikandan, L. Govindarajan, V. Vijayagopal, Prediction of biosorption efficiency for the removal of copper(II) using artificial neural networks, J. Hazard. Mater. 152 (2008) 1268–1275.
[32] V.K. Pareek, M.P. Brungs, A.A. Adesina, R. Sharma, Artificial neural network modeling of a multiphase photodegradation system, J. Photochem. Photobiol., A 149 (2002) 139–146.
[33] S. Aber, N. Daneshvar, S.M. Soroureddin, A. Chabok, K.S. Asadpour-Zeynali, Study of acid orange 7 removal from aqueous solutions by powdered activated carbon and modeling of experimental results by artificial neural network, Desalination 211 (2007) 87–95.
[34] H. Chow, H. Chen, T. Ng, P. Myrdal, S.H. Yalkowsky, Using backpropagation networks for the estimation of aqueous activity coefficients of aromatic organic compounds, J. Chem. Inf. Model. 35 (1995) 723–728.
[35] E.J. Molga, K.R. Westerterp, Neural network based model of the kinetics of catalytic hydrogeneration reactions, Stud. Surf. Sci. Catal. 109 (1997) 379–388.

[36] A.D. Naik, S.S. Bhagwat, Optimization of an artificial neural network for modeling protein solubility, J. Chem. Eng. Data 50 (2005) 460–467.
[37] N. Prakash, S.A. Manikandan, L. Govindarajan, V. Vijayagopal, Prediction of biosorption efficiency for the removal of copper(II) using artificial neural networks, J. Hazard. Mater. (2008) 1268–1275.
[38] A. Aleboyeh, M.B. Kasiri, M.E. Olya, H. Aleboyeh, Prediction of azo dye decolorization by UV/H_2O_2 using artificial neural networks, Dyes Pigm. 77 (2008) 288–294.
[39] J.V. Tu, Advantages and disadvantages of using artificial neural networks versus logistic regression for predicting medical outcomes, J. Clin. Epidemiol. 49 (1996) 1225–1231.
[40] E. Oguz, A. Tortum, B. Keskinler, Determination of the apparent rate constants of the degradation of humic substances by ozonation and modeling of the removal of humic substances from the aqueous solutions with neural network, J. Hazard. Mater. 157 (2008) 455–463.
[41] K. Vasanth Kumar, K. Porkodi, Modelling the solid–liquid adsorption processes using artificial neural networks trained by pseudo second order kinetics, Chem. Eng. J. 148 (2009) 20–25.
[42] N. Bayal, P. Jeevanandam, Synthesis of CuO@NiO core-shell nanoparticles by homogeneous precipitation method, J. Alloys Compd. 537 (2012) 232–241.
[43] A.E.A. Said, M.M.A. El-Wahab, S.A. Soliman, M.N. Goda, Synthesis and characterization of nano CuO–NiO mixed oxides, Nanosci. Nanoeng. 2 (2014) 17–28.
[44] S.A.M. Abdel-Hameed, F.H. Margha, A.A. El-Meligi, Investigating hydrogen storage behavior of $CuMnO_2$ glass-ceramic material, Int. J. Hydrogen Energy 38 (2014) 459–465.
[45] A. Vázquez-Olmos, R. Redón, G. Rodríguez-Gattorno, M. Esther Mata-Zamora, F. Morales-Leal, A.L. Fernández-Osorio, J.M. Saniger, One-step synthesis of Mn_3O_4 nanoparticles: Structural and magnetic study, J. Colloid Interface Sci. 291 (2005) 175–180.
[46] S. Liang, F. Teng, G. Bulgan, R. Zong, Y. Zhu, Effect of phase structure of MnO_2 nanorod catalyst on the activity for CO oxidation, J. Phys. Chem. C 112 (2008) 5307–5315.
[47] L.A. Saghatforoush, M. Hasanzadeh, S. Sanati, R. Mehdizadeh, $Ni(OH)_2$ and NiO nanostructures: synthesis, characterization and electrochemical performance, Bull. Korean Chem. Soc. 33 (2012) 2613–2618.
[48] N. Dharmaraj, P. Prabu, S. Nagarajan, C.H. Kim, J.H. Park, H.Y. Kim, Synthesis of nickel oxide nanoparticles using nickel acetate and poly(vinyl acetate) precursor, Mater. Sci. Eng., B. 128 (2006) 111–114.
[49] G.A. El-Shobaky, N.R.E. Radwan, M. Samy El-Shall, A.M. Turky, H.M.A. Hassan, The role of method of preparation of CuO–NiO system on its physicochemical surface and catalytic properties, Colloids and Surfaces A: Physicochemical and Engineering Aspects 311 (2007) 161–169.
[50] Y.X. Zhang, M. Kuang, J.J. Wang, Mesoporous CuO–NiO micropolyhedrons: facile synthesis, morphological evolution and pseudocapcitive performance, CrystEngComm 16 (2014) 492–498.
[51] G.A. El-Shobaky, N.R.E. Radwan, M.S. El-Shall, A.M. Turky, H.M.A. Hassan, Synthesis and characterization of pure and ZrO_2-doped nanocrystalline CuO–NiO system, Appl. Surf. Sci. 254 (2008) 1651–1660.
[52] F. Yu, Y. Wu, X. Li, J. Ma, Kinetic and thermodynamic studies of toluene, ethylbenzene, and m-xylene adsorption from aqueous solutions onto KOH-activated multiwalled carbon nanotubes, J. Agric. Food Chem. 60 (2012) 12245–12253.
[53] Y.S. Ho, Review of second-order models for adsorption systems, J. Hazard. Mater. B 136 (2006) 681–689.
[54] N.M. Mahmoodi, Nickel ferrite nanoparticle: synthesis, modification by surfactant and dye removal ability, Water Air Soil Poll. 224 (2013) 1419–1429.
[55] N.M. Mahmoodi, Surface modification of magnetic nanoparticle and dye removal from ternary systems, J. Ind. Eng. Chem. 27 (2015) 251–259.
[56] M. Anari-Anaraki, A. Nezamzadeh-Ejhieh, Modification of an Iranian clinoptilolite nano-particles by hexadecyltrimethyl ammonium cationic surfactant and dithizone for removal of Pb(II) from aqueous solution, J. Colloid Interface Sci. 440 (2015) 272–281.
[57] N.M. Mahmoodi, Synthesis of core-shell magnetic adsorbent nanoparticle and selectivity analysis for binary system dye removal, J. Ind. Eng. Chem. 20 (2014) 2050–2058.
[58] N.M. Mahmoodi, Magnetic ferrite nanoparticle–alginate composite: Synthesis, characterization and binary system dye removal, J. Taiwan Inst. Chem. Eng. 44 (2013) 322–330.
[59] N.M. Mahmoodi, S. Khorramfar, F. Najafi, Amine-functionalized silica nanoparticle: Preparation, characterization and anionic dye removal ability, Desalination 279 (2011) 61–68.
[60] N.M. Mahmoodi, B. Hayati, M. Arami, H. Bahrami, Preparation, characterization and dye adsorption properties of biocompatible composite (alginate/titania nanoparticle), Desalination 275 (2011) 93–101.